IEEE Access
Multidisciplinary | Rapid Review | Open Access Journal

Received February 17, 2019, accepted March 4, 2019, date of publication March 8, 2019, date of current version March 29, 2019.

Digital Object Identifier 10.1109/ACCESS.2019.2903765

Dual Mechanical Port Machine Based Hybrid Electric Vehicle Using Reduced Switch Converters

HAMED BIZHANI[1], (Student Member, IEEE), GANG YAO[2], (Member, IEEE), S. M. MUYEEN[3], (Senior Member, IEEE), SYED MOFIZUL ISLAM[4], (Fellow, IEEE), and LAZHAR BEN-BRAHIM[5], (Senior Member, IEEE)

[1]Electrical Engineering Department, University of Zanjan, Zanjan 45371-38791, Iran
[2]Sino-Dutch Mechatronics Engineering Department, Shanghai Maritime University, Shanghai 201306, China
[3]Electrical Engineering Department, Curtin University, Perth, WA 6102, Australia
[4]School of Science, Engineering and Information Technology, Federation University Australia, Melbourne, VIC, Australia
[5]Electrical Engineering Department, College of Engineering, Qatar University, Doha, Qatar

Corresponding author: S. M. Muyeen (sm.muyeen@curtin.edu.au)

This work is supported from Grant No. 61603246 by the National Natural Science Foundation of China.

ABSTRACT Due to the increased environmental pollution, hybrid vehicles have attracted enormous attention in today's society. The two most important factors in designing these vehicles are size and weight. For this purpose, some researchers have presented the use of the dual-mechanical-port machine (DMPM) in hybrid electric vehicles (HEVs). This paper presents two modified converter topologies with a reduced number of switching devices for use on DMPM-based HEVs, with the goal of reducing the overall size and weight of the system. Beside the design of the DMPM in the series-parallel HEV structure along with the energy management unit, the conventional back-to-back (BB) converter is replaced with nine-switch (NS) and five-leg (FL) converters. These converters have never been examined for the DMPM-based HEV, and therefore, the objective of this paper is to reveal the operational characteristics and power flow mechanism of this machine using the NS and FL converters. The simulation analysis is carried out using MATLAB/Simulink considering all HEV operational modes. In addition, two proposed and the conventional converters are compared in terms of losses, maximum achievable voltages, required dc-link voltages, the rating of the components, and torque ripple, and finally, a recommendation is made based on the obtained results.

INDEX TERMS Back-to-back converter, dual mechanical port machine, five-leg converter, hybrid electric vehicle, nine-switch converter.

I. INTRODUCTION

Due to the environmental issues and the limited resources of the fossil fuels, the use of zero-emission or low emission vehicles like electric vehicles (EVs) and hybrid vehicle (HV) technologies is increasing nowadays [1]. A hybrid vehicle that includes an internal combustion engine (ICE) and an electric motor is called hybrid electric vehicle (HEV). According to various configurations, the HEVs can be divided into three categories: series, parallel, and series-parallel schemes [2]. In the series-parallel HEVs, the mechanical operating points (torque and speed) of the ICE and the wheels characteristics are autonomous. Therefore, the ICE can be controlled to operate in the high-efficiency region of its characteristic. With the operation of the ICE in this region, the minimum fuel consumption of the vehicle can be guaranteed [3]. Moreover, in a series-parallel structure, the ICE can deliver most of its power to the wheels without multi-stage conversion. The earlier feature is due to the parallel part of the series-parallel structure, while the later one is due to its series nature [3], [4]. The overall performance of the series-parallel HEV is such that, when the ICE efficiency is low in the starting and braking modes, the vehicle's drive system decouples the ICE and the vehicle is driven out by the electric motor connected to the wheels, powered by the battery. This strategy allows the ICE to link with the wheels only when its efficiency is high. In this case, the vehicle's efficiency will increase and the fuel consumption and pollution will decrease as well. Despite this optimal performance, there are still some disadvantages in the HEVs

The associate editor coordinating the review of this manuscript and approving it for publication was Tariq Masood.

structure. In particular, the implementation of above system requires one additional electrical machine and a mechanical version of a continuous variable transmission (CVT) called planetary gear set to link the ICE and both electrical machines to the wheels [5]. These requirements increase the weight, size, frictional losses, audible noise, and maintenance cost of the HEVs [6]. To overcome these requirements, researchers proposed Dual Mechanical Port Machine (DMPM) as an alternative [7], [8]. Due to the structure of the DMPM, it can operate as a motor and a generator. In addition, there is no need for a planetary gear, because the DMP machine is an electrical variable transmission (EVT). As a result, the size and cost of the system will be reduced [9]. Considering the main concept of the EVT, different types of modified DMPM has been reported in literature [10]–[15]. In [10] and [11], the single-layer squirrel cage outer rotor based DMP machine (SCDMP) is presented. Since the PM is removed from the inner rotor, compared with the first version of the DMPM, the cost of the machine reduces and the thermal robustness increases. A hybrid excitation on the single layer of the PM based EVT consists of a PM and a dc-field winding is reported in [12]. The later excitation regulates the stator flux linkage to minimize the iron and copper losses in the machine at the same time by optimal control of the dc current. In [13], a novel brushless dual mechanical port flux–switching PM (BDMP-FSPM) is presented for a plug-in HEVs. In that paper, a non-contact magnetic planetary gear (NC-MPG) is used instead of the mechanical version of the CVT. Since the internal gap of the motor is completely utilized, the overall size of the motor is reduced and the power and torque density can be further improved. A new magnetic field-modulated brushless dual rotor machine (MFM-BDRM) and its speed, torque, and power characteristic of the speed, torques, and power were analyzed in [14] and [15].

Another crucial issue related to both EVs and HEVs is the required power electronic converters in order to interface different electrical parts. In hybrid electric vehicles based on the independent motor and generator, there is a need for the bidirectional six-switch converter for each machine along with a DC-DC converter as an interface between battery and DC-link [16]–[18]. Various types of DC-DC converters, which are mostly appropriate options for EVs, have been investigated in previous research works [19]–[21]. In [19] an interface topology suitable for charging the batteries of an EV is reported. That converter is able to provide both buck and boost modes as well as the power factor correction. A modified non-isolated single-inductor multiple-input buck DC–DC converter, which can be considered as an appropriate choice for hybrid dc sources based pure electric vehicle is addressed in [20]. For same application, a multi-input DC-DC interface, which is able to integrate three DC-sources such as photovoltaic (PV) system, fuel cell (FC), and energy storage system (ESS), is presented in [21]. Unlink the DC-DC conversion systems, which have experienced many improvements, DC-AC conversion parts of EV/HEVs have not been strongly explored in previous literature. An integrated multilevel converter of switched reluctance motors (SRMs) supplied by a modular front-end circuit for plug-in hybrid electric vehicle (PHEV) applications is developed in [22]. In [23], the nine-switch (NS) converter is used to supply two electrical machines that play roles of the motor and generator in the HEV for simple modes. That paper does not use the real dynamic model of the vehicle (merely used two machines to show the HEV performance), the energy management unit, and the standard driving cycle. In [24], a five-leg power electronic interface is used to drive two permanent magnet synchronous machines (PMSM) in order to independent control of wheels in EV application. An indirect matrix converter (IMC) structure for HEV applications with three-phase and single-phase outputs is reported in [25]. For the DMPM-based HEVs, researchers have not focused on the power electronic converters, therefore, simply used the back-to-back (BB) converters which require 12 switches for the energy conversion [2], [3], [7], [8].

Considering the capability of the NS and FL converters for simultaneous supplying of two independent three-phase loads [26]–[29], in this work, the conventional back-to-back converter used in the DMPM-based HEV is replaced with these converters in order to reduce the volume and cost by lowering the use of the semiconductor components and their accessories. Indeed, the innovation of this work is the combination of both EVT and NS/FL converters in order to reduce the size of the HEV as much as possible. With these converters, two outputs can be fed properly, the HEV can be operated well in the operational modes of the standard drive cycle, and the weight and the overall size of the system might be reduced.

II. DMPM BASED HEV

A. DMPM OPERRATION PRINCIPLE

The DMP machines are a new generation of the electric machines with two mechanical ports and two electric ports. As shown in the Fig. 1, these machines consist of two rotors and one stator. The stator is one of the electrical ports and has a three-phase winding. The outer rotor consists of a permanent magnet (PM) that composes a permanent magnet synchronous motor (PMSM) with the stator. The inner rotor also has a three-phase winding and is powered by a

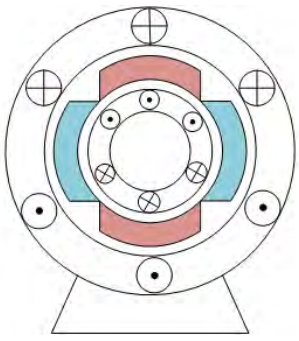

FIGURE 1. DMP machine structure.

brush and a slider ring. This rotor includes an electric port and a mechanical port, and it forms a double-fed induction generator (DFIG) with stator [2]. The electric port on the inner rotor balances the energy of the machine. It should be noted that the PM rotor could receive power from both electric parts. In fact, the torque and power in the air gap between the inner rotor, PM and stator are exchanged for the energy balancing purpose. In general, two independent inverters, which are connected back-to-back to a DC bus, are used to feed two electric ports. Depending on the relative speed of the two rotors, the DMP machine might experience different states [30]. The dynamic equations of the machine in the dq0 reference frame, which is rotated synchronously with the PM rotor, can be expressed as follows [2]. It is noted that since the performance of the proposed converters is the main aim of this paper, the simple dq0 model is considered.

$$V_{qs} = i_{qs}r_s + d\lambda_{qs}/dt + \omega\lambda_{ds} \quad (1)$$
$$V_{ds} = i_{ds}r_s + d\lambda_{ds}/dt - \omega\lambda_{qs} \quad (2)$$
$$V_{qr} = i_{qr}r_r + d\lambda_{qr}/dt + (\omega - \omega_r)\lambda_{dr} \quad (3)$$
$$V_{dr} = i_{dr}r_r + d\lambda_{dr}/dt - (\omega - \omega_r)\lambda_{qr} \quad (4)$$
$$\lambda_{qs} = L_s i_{qs} + L_m i_{qr} \quad (5)$$
$$\lambda_{ds} = \lambda_m + L_s i_{ds} + L_m i_{dr} \quad (6)$$
$$\lambda_{qr} = L_r i_{qr} + L_m i_{qs} \quad (7)$$
$$\lambda_{dr} = \lambda_m + L_r i_{dr} + L_m i_{ds} \quad (8)$$

where L_s and L_r, are self-inductances of the stator and inner rotor windings, r_s and r_r are resistors of the stator and inner rotor windings, L_m is mutual inductance between the inner rotor and stator windings. λ_{m1} and λ_{m2} are the flux linkages produced by the PM-rotor in the outer and inner machines respectively, ω is outer rotor speed, and ω_r is inner rotor speed. The electromagnetic torque developed on outer and inner rotors are respectively defined in [2] as (9) and (10). Considering applied torque by ICE and imposed torque by wheels, the dynamic equations between different masses can be written as (11) and (12).

$$\begin{aligned} T_{out} = p\Big[&\sqrt{3/2}\left(i_{qs}\lambda_{m1} + i_{qr}\lambda_{m2}\right) \\ &+ 3/2\left(L_{sd} - L_{sq}\right) i_{ds} i_{qs} \\ &+ 3/2\left(L_{rd} - L_{rq}\right) i_{dr} i_{qr} \\ &+ 3/2\left(L_{md} - L_{mq}\right)\left(i_{sd} i_{qr} + i_{qs} i_{dr}\right)\Big] \end{aligned} \quad (9)$$

$$\begin{aligned} T_{in} = -p\Big[&\sqrt{3/2}\, i_{qr}\lambda_{m2} + 3/2 L_{md} i_{ds} i_{qr} \\ &- 3/2 L_{mq} i_{qs} i_{dr} - 3/2\left(L_{qr} - L_{dr}\right) i_{dr} i_{qr}\Big] \end{aligned} \quad (10)$$

$$T_{ICE} - T_{in} = J_{im} + d\omega_{in}/dt + B\omega_{in} \quad (11)$$
$$T_{out} - T_{Load} = J_{out} + d\omega_{out}/dt + B\omega_{out} \quad (12)$$

where T_{out} and T_{in}, T_{ICE}, and T_{load} are the PM rotor, inner rotor, ICE and load torques, respectively. J_{in}, J_{out}, ω_{in}, and ω_{out} are the inertia and speed of the inner and PM rotors, respectively, and p is the number of the pole pairs.

B. DMPM APPLICATION IN HEVs

Fig. 2 shows the general mechanical section of a DMPM-based HEV. As it is shown, in a DMP-based HEV, the PM and inner rotors link to the wheels and ICE, respectively. In addition, due to the magnetic couplings of the different parts, there is no need for a planetary gear to synchronize them, which is most salient feature of this EVT.

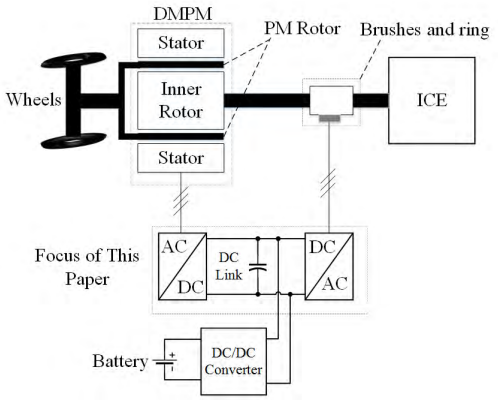

FIGURE 2. DMPM based HEV structure.

C. ENERGY MANAGEMENT OF DMPM BASED HEV

In general, demanded torque by the vehicle might be provided through two parts. One part is due to the interaction of the inner rotor and PM fields (T_{in}) and the other one is through the interaction between the stator and PM fields (T_{out}). When the ICE is turned on, its torque is converted to a negative torque between the PM and the inner rotor due to the interaction of their fields. This negative torque causes a current flow from the inner rotor winding to the battery. This power is then given to the stator windings and creates a stator field. Finally, the interaction of this field with the PM field applies a positive torque on the PM rotor and the wheels. The operating modes of a HEV can be classified as 1: Start-up, 2: Normal mode, 3: Acceleration, 4: Battery charge and 5: Braking. Assuming that the ICE operates at the high efficiency region, the probable states for the vehicle are examined as follows [30].

1- The first state is the start-up mode. In this mode, the ICE is turned off for optimal efficiency, and the battery will start up the vehicle.

2- The second state is related to the acceleration mode. In this mode, the ICE is linked to the PM rotor and provides the larger part of the requested power by the vehicle. The other part of this power is provided by the battery and through the stator. In this mode, the battery is discharged.

3- The third state refers to the normal vehicle condition. In this mode, the demanded power by the vehicle is less than or equal to the ICE's power. If the ICE's power is higher than the demanded power, the excess power can be stored in the battery through the stator.

4- The fourth state is when the vehicle is in the recharge mode. In this mode, the ICE is responsible to provide the requested power by wheels as well as the required power for

recharging of the battery. When the state of charge (SOC) of the battery is lower than the specified value, which is 40% in this paper, this mode will be activated.

5- The fifth state refers to the braking mode. In this mode, the acceleration value is negative, so the kinetic energy of the wheels (PM rotor) is recovered and stored in the battery. In this mode, the ICE should be switched off.

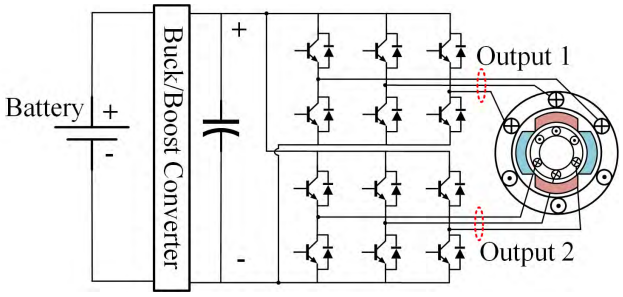

FIGURE 3. DMPM based HEV with BB converter (conventional).

III. PROPOSED CONVERTERS FOR DMPM BASED HEV

In conventional hybrid electric vehicles (including the DMPM-based HEVs), the BB converter topology shown in Fig. 3 is used for the bidirectional supply. As shown, each winding has its own converter, which means 12 switches are totally needed. In this study, two well-known converters with a reduced number of switches named nine-switch and five-leg converters are introduced and adopted for use in the structure of the DMPM-based HEV. Unlike the BB converter in which there is no shared part between outputs, in NS and FL converters the outputs are in common through a few switches as shown in Fig. 4 and Fig. 5. Compared to the BB converter, the NS and FL converters have three and two fewer switches than the BB converter, respectively. It should be noticed that as conventional DMPM-based HEVs, a buck/boost DC-DC interface should be used between battery and DC terminal of the converters in order to regulate the DC link voltage as well as reducing the number required battery modules.

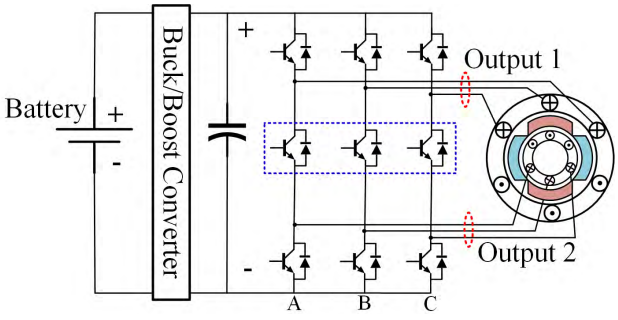

FIGURE 4. DMPM based HEV with NS converter (proposed).

IV. DMPM BASED HEV MODELING

A. ENERGY MANAGEMENT SYSTEM MODELING

The identification procedure of the operation mode of the vehicle is shown in Fig. 6 [2], where the mentioned modes

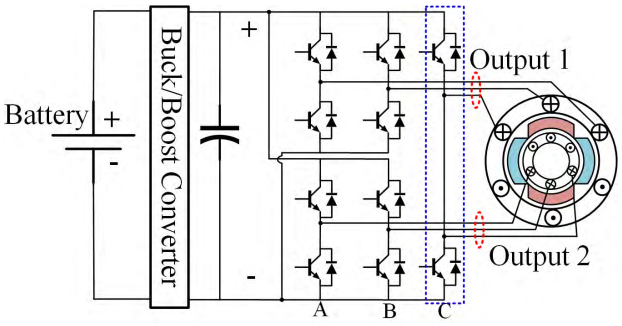

FIGURE 5. DMPM based HEV with FL converter (proposed).

```
1. Enter the acceleration, vehicle speed and SOC values.
2. Use the lookup table of the torque-speed characteristic of the
   vehicle to calculate the maximum availabe torque.
3. Calculate the requested drive power.
4. Calcluate the operational mode
   If acc > 0
      If SOC < 0.4
         While 0.4 ≤ SOC ≤ 0.8
            Mode = 4;
         End
      Else
         If drive power < 11kW
            If vehicle speed < 10km/h
               Mode = 1;
            Else if acc < 0.5
               Mode = 3;
               End
            End
         Else if acc > 0.5
               Mode = 2;
               End
         End
      End
   Else
      Mode = 5;
   End
5. Calculate the ICE's power and its refernce speed based on its
   efficiency characterestic lookup table
6. Calculate the refernce torque for the stator
```

FIGURE 6. Pseudo code of energy management unit.

are related to vehicle states described in Sec.II.C. Initially, the acceleration, which is equivalent to the gas pedal position pressed by the driver, along with the vehicle speed and SOC of the battery are measured. Then, according to the torque-speed characteristic of the vehicle, the maximum available torque in corresponding vehicle speed along with requested power by vehicle are calculated. Next, considering the applied constraints, the operation mode of the vehicle is obtained. Finally, regard to the operation mode of the vehicle and the efficiency characteristic of the ICE, the reference speed and torque of the ICE along with reference powers, which must be injected by ICE and battery, are calculated. If the ICE operates in this reference speed, its performance on the optimal line in efficiency curve can be guaranteed. The numbers assigned to the modes in Fig. 6 are related to the operational modes classified in section II.C. It should be noticed that in order to

reduce the depth of charging/discharging of the battery and consequently, increase the life span of the battery, the lower and upper boundaries for SOC are respectively restricted to 40% and 80% [2].

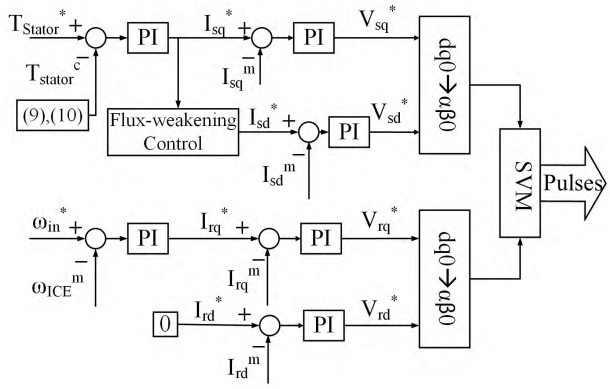

FIGURE 7. Control strategy.

B. CONTROL STRATEGY

The control strategy used in this paper is shown in Fig. 7. As shown, the torque provided by the stator is calculated and compared to the reference value given by the energy management unit. The torque error is progressed through a proportional-integrator (PI) controller to generate the reference value for the q-axis stator current. At speeds less than the nominal speed, in order to achieve the maximum torque per current and the minimum current loss, the reference value for the d-axis current is set zero [2], [3]. In this condition, the torque only is controlled by i_{qs}. At the speeds above the nominal speed, however, as the electromotive force increases and the control of the vehicle is become difficult, a flux-weakening strategy is used [2], [32]. Therefore, the value of the i_{ds} is set to a negative value depending on the nominal current of the machine to create the flux-weakening effect. In practice, however, the permanent magnets can be demagnetized since the value of the d-axis flux is in opposition to the PM flux [33], [34]. On the other hand, the actual speed of the inner rotor is measured and compared to the reference value given by the energy management unit and is given to the PI controller. The output of the PI controller is the reference current of the q-axis of the inner rotor winding i_{qr}. According to the usage of the synchronous frame theory for the control strategy, the torque is controlled only by the q-axis current. Therefore, the reference current of the d-axis is zero. Then, the currents of the d and q axes for the stator and rotor are compared with the measured values of their respective currents. Finally, the difference between them passes through a PI controller to obtain the stator and the rotor reference voltages.

C. SPACE VECTOR MODULATION

1) SVM FOR CONVENTIONAL BB CONVETER

In a six-switch converter, in general, we have 32 switching states depending on the positions of the three top switches of each leg. By removing the undefined states, six active vectors and two zero vectors, as shown in Fig. 8, are remained. In each switching cycle, according to the reference voltage obtained from the control section, the corresponding sector is firstly identified. Then the reference vector is constructed using its adjacent vectors and based on the time length for each adjacent vector, which can be calculated using the following expressions.

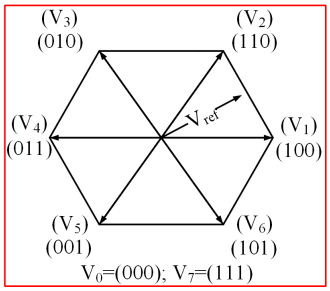

FIGURE 8. Active vectors of BB converter in polar frame.

$$t_1 = \sqrt{3}/2mt_s \sin(\pi/3 - \alpha) \tag{13}$$

$$t_2 = \sqrt{3}mt_s \sin(\alpha) \tag{14}$$

$$t_0 = t_s - t_1 - t_2 \tag{15}$$

$$m = V_{ref}/V_{dc} \tag{16}$$

where t_1, t_2, and t_0 are the time lengths of the first adjacent, the second adjacent and zero vectors, respectively. t_s is switching period, m is modulation index, α is the angle of the reference voltage, V_{ref} is the magnitude of the reference voltage and V_{dc} is the voltage of the DC link.

It should be noticed that there is a freedom in selection of the type and position of the zero vectors in the vectors sequence. The sequence of vectors must be so that the least change in the status of the switches and consequently in the switching losses can be achieved.

TABLE 1. On and off status of switches located in each leg.

	S_{IU}	S_{IM}	S_{IL}
1	ON	OFF	ON
2	OFF	ON	ON
3	ON	ON	OFF

2) SVM FOR PROPOSED NS CONVERTER

In this converter, since two AC outputs are common in three intermediate switches, it is somewhat difficult to control the load autonomously [23]. To overcome this limitation, this paper uses a sequential switching method [23]. In this method, for independent performance of two outputs, a part of the switching period is assigned to the first output and the rest for the second output. The zero vectors are also divided between two outputs. The different states for each leg are shown in Table 1. U, M, and L are subscripts for the upper, middle, and lower switches of each leg, respectively.

TABLE 2. Switching states for nine switch converter.

Switching Number	A	B	C	Output 1	Output 2
1	3	3	3	Zero	Zero
2	3	3	1	Zero	Active
3	3	1	1	Zero	Active
4	1	1	1	Zero	Zero
5	1	1	2	Active	Zero
6	1	2	2	Active	Zero
7	1	2	1	Active	Zero
8	2	2	1	Active	Zero
9	2	1	1	Active	Zero
10	2	2	2	Zero	Zero
11	2	1	2	Active	Zero
12	1	1	3	Zero	Active
13	1	3	3	Zero	Active
14	1	3	1	Zero	Active
15	3	1	3	Zero	Active
16	2	2	3	Active	Active
17	2	3	3	Active	Active
18	2	3	2	Active	Active
19	3	3	2	Active	Active
20	3	2	2	Active	Active
21	3	2	3	Active	Active

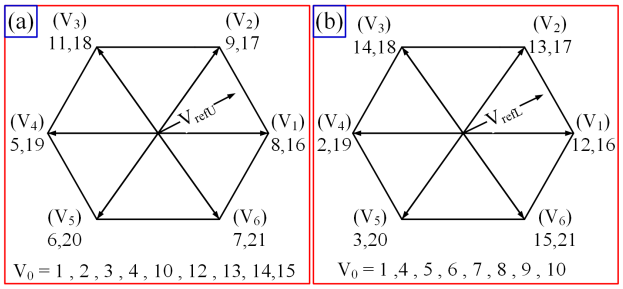

FIGURE 9. Active vectors of NS converter in polar frame, (a) upper output and (b) lower output.

In general, this converter has 21 valid switching states as show in Table 2. Fig. 9 shows the active vectors of the first and second outputs in polar coordinate. In this converter, sector which the reference vector of each output is located, should be firstly calculated. Then, the adjacent vectors of each reference vector must be identified and switched to a specific time for each output. The time length assigned to each vector is calculated as following.

$$t_1 = \sqrt{3}/2 m_U t_s \sin(\pi/3 - \alpha_U) \quad (17)$$

$$t_2 = \sqrt{3}/2 m_U t_s \sin(\alpha_U) \quad (18)$$

$$t_3 = \sqrt{3}/2 m_L t_s \sin(\pi/3 - \alpha_L) \quad (19)$$

$$t_4 = \sqrt{3}/2 m_L t_s \sin(\alpha_L) \quad (20)$$

$$t_0 = t_s - t_1 - t_2 - t_3 - t_4 \quad (21)$$

$$m_U = 2V_{refU}/V_{dc} \quad (22)$$

$$m_L = 2V_{refL}/V_{dc} \quad (23)$$

where t_1, t_2, t_3, t_4, and t_0 are switching times of the first adjacent vector of the first output, the second adjacent vector of the first output, the first adjacent vector of the second output, the second adjacent vector of the second output and zero vector, respectively. m_U and m_L are the modulation indexes of the upper and lower outputs, α_U and α_L are angles of the reference voltages of the upper and the lower outputs, V_{refU} and V_{refL} are magnitudes of the reference voltages of the upper and the lower outputs and V_{dc} is the voltage of the DC link.

TABLE 3. Switching states for five leg converter.

Switching Number	State of upper switches of each leg	First output	Second output
1	00000	Zero	Zero
2	00001	Active	Active
3	00010	Zero	Active
4	00011	Active	Active
5	00100	Zero	Active
6	00101	Active	Active
7	00110	Zero	Active
8	00111	Active	Zero
9	01000	Active	Zero
10	01001	Active	Active
11	01010	Active	Active
12	01011	Active	Active
13	01100	Active	Active
14	01101	Active	Active
15	01110	Active	Active
16	01111	Active	Zero
17	10000	Active	Zero
18	10001	Active	Active
19	10010	Active	Active
20	10011	Active	Active
21	10100	Active	Active
22	10101	Active	Active
23	10110	Active	Active
24	10111	Active	Zero
25	11000	Active	Zero
26	11001	Zero	Active
27	11010	Active	Active
28	11011	Zero	Active
29	11100	Active	Active
30	11101	Zero	Active
31	11110	Active	Active
32	11111	Zero	Zero

3) SVM FOR PROPOSED FL CONVERTER

In this converter, two outputs are common in one leg [28], which makes it difficult to control the load independently. However, this problem will be fixed by using the sequential switching for this converter as well. This converter has 32 acceptable switching states as shown in Table 3. These 32 switching states make 32 vectors in a polar frame for both outputs, including 24 active vectors and 8 zero vectors. Among these vectors, 12 vectors are individual vectors, which create active vector in one of the outputs while create a zero vector for another output. Fig. 10 illustrates these active and zero vectors for both outputs in the polar frame. Like two previous converters, in this converter, the adjacent vectors are identified after determining the sector in which the reference

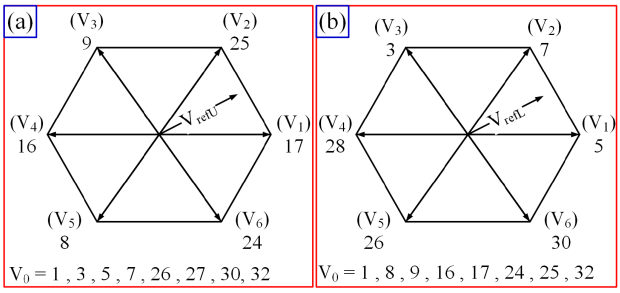

FIGURE 10. Active vector of FL converter in polar frame, (a) upper output and (b) lower output.

vector of each output is located. The time assigned to each adjacent vector can be calculated by (17) to (23), which were used for NS converter.

V. COMPONENT REQUIERMENTS

A. DC LINK VOLTAGE

As it is mentioned earlier, in sequential switching method used in NS and FL converters, the switching period is divided in two parts depending on the amplitude and phase of the reference voltages. This means unlike the BB converter in which the DC-link energy is simultaneously available for both outputs, in NS and FL converters, each output is connected to the DC-link only for a fraction of the switching period. Therefore, in order to achieve same voltages at the outputs of the NS and FL converters in comparison with the BB converter, higher DC-link voltage should be used. Considering the time lengths assigned to the adjacent vectors, which in total should be equal or less than the switching period, the required value for DC-link voltage in NS and FL converters can be calculated as follow:

$$t_1 + t_2 + t_3 + t_4 \leq t_s \tag{24}$$

Considering (17) – (20), it can be re-written as:

$$\sqrt{3}/2 t_s \left(m_U \left(\sin\left(\pi/3 - \alpha_U\right) + \sin\left(\alpha_U\right)\right) + m_L \left(\sin\left(\pi/3 - \alpha_L\right) + \sin\left(\alpha_L\right)\right)\right) \leq t_s \tag{25}$$

Eq. (25) is maximum when:

$$\alpha_i = \pi/6, \quad i = U, L \tag{26}$$

Substituting (26) into (25) yields:

$$\sqrt{3}/2 \left(m_U + m_L\right) \leq 1 \tag{27}$$

Considering (22) and (23):

$$\sqrt{3} \left(V_{refU} + V_{refL}\right) \leq V_{dc} \tag{28}$$

From (28), in order to have the same maximum achievable output voltages, larger DC-link voltage is required in the NS and FL converters compared to the BB converter. This means, with the same DC-link voltage, the maximum achievable voltages in NS and FL converters would be less than the BB converter.

B. POWER SWITCHING RATING

In order to compare the rating of the power electronic components in different topologies, the current flow paths at different operational modes should be analysed. Unlike the BB converter, in which stator and rotor side converters have independent current flow paths, in the NS and FL converters depending on the operational modes, current might pass through some common switches between stator and rotor side converters. As it is shown in Fig. 11(a), switches located in upper and lower ports of the BB converter experience stator and rotor side currents, respectively. This means the rating of these switches depend on the rated current of the stator and rotor windings, which might pass through.

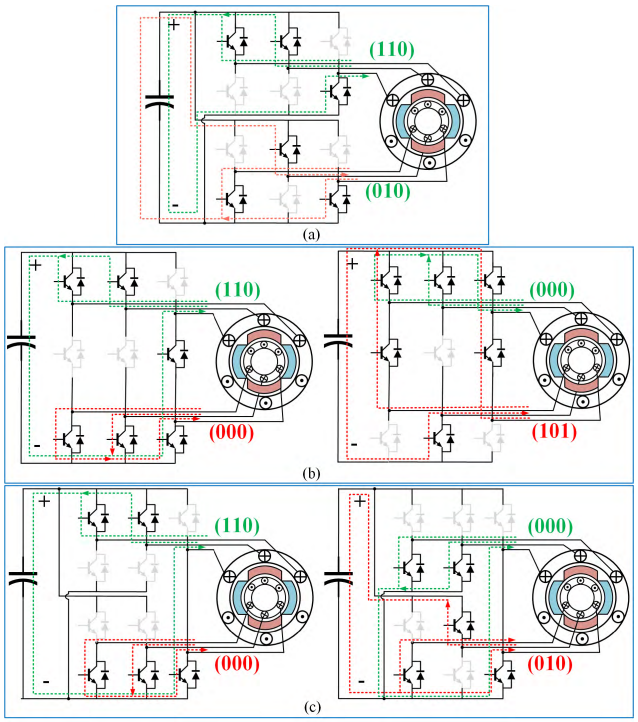

FIGURE 11. Current flow paths for different converters, (a) BB, (b) NS, and (c) FL.

For NS converter, switches would experience different currents depending on the applied vectors to the upper and lower ports, as shown in Fig. 11(b). In DMPM based HEV applications, the upper and lower ports can be connected to the stator and rotor windings, which may operate as source or load. Therefore, in order to determine the rating of the switches, all five operational modes of the DMPM based HEV mentioned in section II.C, must be considered. Instantaneous currents flowing through the switches located in leg A are shown in Fig. 12(a). The rating of the middle switches can be determined from the maximum current between i_s and i_r. On the other hand, for the top and bottom switches, sum of the stator and rotor currents should be considered. Depending on the operational modes, these currents could have different specifications as summarized in Table 4. Since the stator and rotor side ports experience different frequencies, the maximum

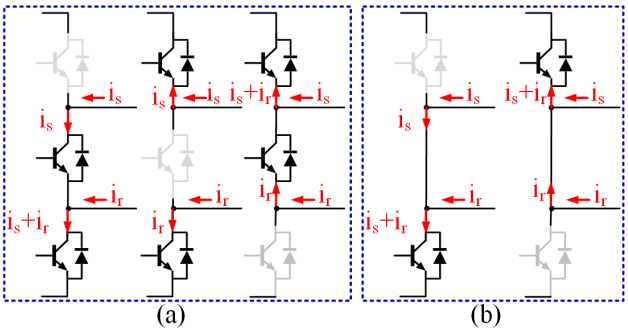

FIGURE 12. Flowing currents through the switches in (a) NS and (b) FL.

TABLE 4. Stator and rotor windings' specifications.

Operational Modes			Frequency	Amplitude	Type
Start-up		$i_{w\text{-}s}$	ω_{HEV}	$\propto P_{HEV}$	Load
		$i_{w\text{-}r}$	ω_{HEV}	0	Source
Normal	$T_{ICE}<T_{HEV}$ $\omega_{ICE}>\omega_{HEV}$	$i_{w\text{-}s}$	ω_{HEV}	$\propto \Delta T$	Load
		$i_{w\text{-}r}$	ω_{slip}	$\propto \omega_{slip}$	Source
	$T_{ICE}>T_{HEV}$ $\omega_{ICE}<\omega_{HEV}$	$i_{w\text{-}s}$	ω_{HEV}	$\propto \Delta T$	Source
		$i_{w\text{-}r}$	ω_{slip}	$\propto \omega_{slip}$	Load
Acceleration		$i_{w\text{-}s}$	ω_{HEV}	$\propto \Delta T$	Load
		$i_{w\text{-}r}$	ω_{slip}	$\propto \omega_{slip}$	Load
Recharge		$i_{w\text{-}s}$	ω_{HEV}	$\propto \Delta T$	Source
		$i_{w\text{-}r}$	ω_{slip}	$\propto \omega_{slip}$	Source
Braking		$i_{w\text{-}s}$	ω_{HEV}	$\propto P_{HEV}$	Source
		$i_{w\text{-}r}$	ω_{HEV}	0	Source

* T_{ICE} and ω_{ICE} are mechanical torque and speed of the ICE. P_{HEV}, T_{HEV} and ω_{HEV} are requested power, requested torque and mechanical speed of the HEV, ω_{silp} is slip speed between inner and outer rotors, and ΔT is equal to T_{HEV}-T_{ICE}.

current that should be selected for the current rating of the bottom and top switches is equal to $I_{smax} + I_{rmax}$ [35], [36].

Same justification can be used for switches in shared leg of the FL converter as shown in Fig. 11(c). The maximum current that would pass through the both switches is $i_s + i_r$, as shown in Fig. 12(b). Considering Table 4, the current rating of these switches would be $I_{smax} + I_{rmax}$. For individual legs of FL converter, the current rating of the switches can be determined like BB converter. Components requirement for different topologies is summarized in Table 5, where $I_{w-srated}$ and $I_{w-rrated}$ are nominal currents of the stator and inner rotor windings, respectively.

C. LOSS COMPARISON

In BB converter, switches pass stator current or inner rotor current at any moment of the time. Therefore, the loss calculation of this converter can be performed easily. However, in NS and FL converters, the switches might experience stator current or rotor current or both, making the switching loss calculation complicated. Therefore, in this paper, the switching loss comparison is performed approximately. Referred to [23], the switching loss for different topologies can be summarized as Table 5, where E_{ON} and E_{OFF} are wasted energy while switches are being turned ON and OFF, and E_{rr} is wasted energy when diode is being turning OFF with current I_n and voltage V_n. For this purpose, the same operational mode and same transition states (100 to 011 for both outputs) are applied to the different topologies. Then, in order to calculate the switching loss, the instantaneous currents, which should be interrupted and conducted by each switch during the two sequential switching periods, is identified. As it is shown in Table 5, the switching loss of the NS and FL converters can be less than BB converter depending on the nominal currents of the stator and inner rotor windings. However, due to the use of higher DC-link voltage in these topologies, the switching loss reduction caused by currents might be neutralized.

Considering same specifications for switches in different topologies, the conduction loss is proportional to the instantaneous current flowing through the switches [35], [36]. For BB converter, the instantaneous currents of the upper and lower ports are related to the currents of stator and rotor windings. In NS converter, as shown in Fig. 12(a), the upper and lower switches might experience instantaneous currents more or less than the BB converter's currents, depending on the amplitude, polarity and frequency of the stator and rotor currents. The individual legs of FL converter would have the same currents as BB converters, although the switches located in shared leg might experience instantaneous currents less or more than the BB converter.

VI. SIMULATION VALIDIATION USING STANDARD DRIVING CYCLE

For effective analysis of the proposed structures, a standard drive cycle that contains all operating modes of the HEV is considered. For this aim, using the U. S. Department of energy (DOE) report [37], which examines the Toyota Prius, this standard drive cycle for simulation with same parameters as [2], is derived as shown in Fig. 13(a). From Fig. 13(b) it can be seen that the required torque of the wheels is proportional to the input acceleration. In the braking mode, this torque is negative. To obtain the amount of the power required by the vehicle at the desired speed and the acceleration, simply multiply the mechanical speed of the vehicle in radians per second by the torque obtained in the previous section (See Fig. 14(b)). As it can be seen in Fig. 14(a), the vehicle's

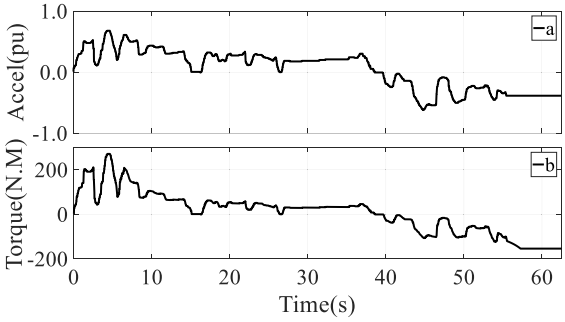

FIGURE 13. Simulation results, (a) standard drive cycle based on DOE report, and (b) requested torque by wheel.

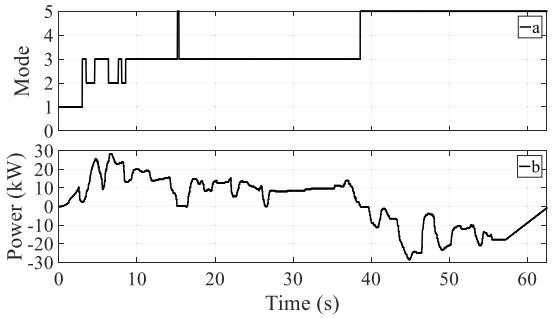

FIGURE 14. Simulation results, (a) operational mode of HEV based on energy management unit, and (b) requested power by vehicle.

operating modes might vary from 1 to 5, as described in section II.C.

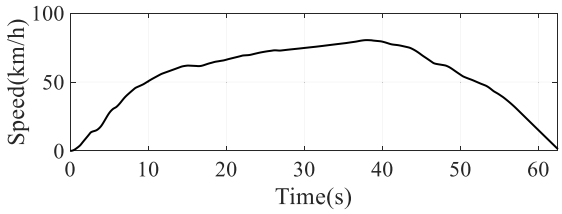

FIGURE 15. Vehicle speed.

As it is shown in Fig. 15, when the acceleration and the torque are positive, the velocity increases and in the braking modes (moments when acceleration are negative) the velocity decreases. In comparison with the results presented in [37], which is the related results for the vehicle speed in DOE report, the accuracy of the results obtained from DMP-based HEV in presence of BB, NS, and FL converters can be verified. It should be noticed that since the results of the vehicle speed and the operational modes are the same in three scenarios, only one of them has been mentioned in this section.

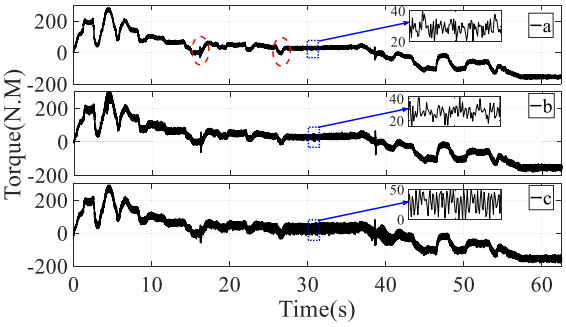

FIGURE 16. Applied torque to wheels, (a) BB, (b) NS, and (c) FL converters.

According to Fig. 16, it can be seen that the vehicle works well in the presence of all three converters and follows the reference torque. The areas indicated with the red doted circles in Fig. 16(a) show the moments when the acceleration is close to zero, and therefore the output torque goes to zero. As it is

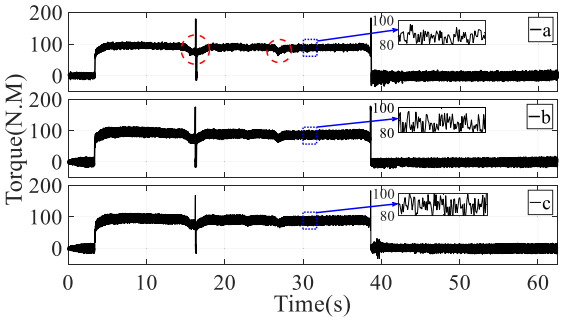

FIGURE 17. Applied torque from ICE to wheels, (a) BB, (b) NS, and (c) FL converters.

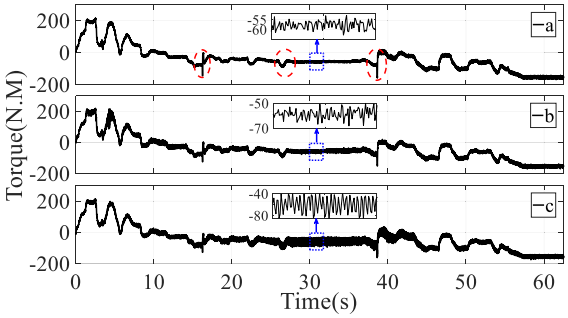

FIGURE 18. Applied torque from the stator to wheels, (a) BB, (b) NS, and (c) FL converters.

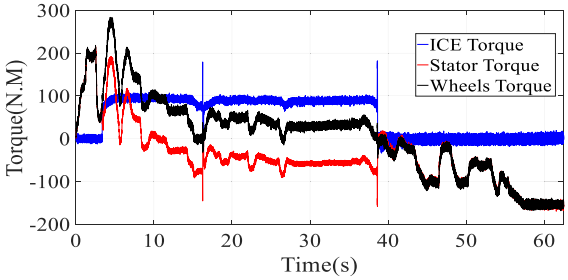

FIGURE 19. All generated torques for BB converter in one frame.

depicted in Fig. 17, the ICE is off at the beginning of the drive cycle in accordance with the operating modes. Gradually by accelerating the vehicle and reaching to a certain speed and power, the ICE is linked and provides larger part or all of the requested power by the vehicle. In the areas indicated with the red doted circles in Fig. 17(a) since the acceleration is negative for a short time, the ICE is turned off. As the speed of the vehicle has not been reduced, the ICE re-lights up as the acceleration progresses. As shown in Fig. 18, the stator torque is positive in modes 1 and 2, where the battery can be pulled up, and in the mode 5, which is a braking mode, the power flows from the wheels to the battery, the stator torque is negative. The points highlighted in Fig. 18(a) are the moments in which the stator torque is affected by the ICE ignition. In time interval between 10 to 38 seconds (mode 3) in which the requested torque by the vehicle is less than the applied torque by the ICE, in order to maintain the ICE in the

TABLE 5. Comparison of different topologies.

	Switching Loss	Power rating of the switches	Required DC-link Voltage
BB	$\frac{f_s}{\pi}\left(E_{ON}+E_{OFF}+E_{rr}\right)\left(6I_{w-s}^{rated}+6I_{w-r}^{rated}\right)\frac{V_{dc}}{V_nI_n}$	$6I_{w-s}^{rated}+6I_{w-r}^{rated}$	$\sqrt{3}\times\max\left\{V_{refU},V_{refL}\right\}$
NS	$\frac{f_s}{\pi}\left(E_{ON}+E_{OFF}+E_{rr}\right)\left[4I_{w-s}^{rated}+6I_{w-r}^{rated}+4\left(\left\|I_{w-s}^{rated}\right\|-\left\|I_{w-r}^{rated}\right\|\right)\right]\frac{V_{dc}}{V_nI_n}$	$3\times\max\left\{I_{w-s}^{rated},I_{w-r}^{rated}\right\}+6\left\{I_{w-s}^{rated}+I_{w-r}^{rated}\right\}$	$\sqrt{3}\times\left(V_{refU}+V_{refL}\right)$
FL	$\frac{f_s}{\pi}\left(E_{ON}+E_{OFF}+E_{rr}\right)\left[5I_{w-s}^{rated}+5I_{w-r}^{rated}+\left(\left\|I_{w-s}^{rated}\right\|-\left\|I_{w-r}^{rated}\right\|\right)\right]\frac{V_{dc}}{V_nI_n}$	$4I_{w-s}^{rated}+4I_{w-r}^{rated}+2\left\{I_{w-s}^{rated}+I_{w-r}^{rated}\right\}$	$\sqrt{3}\times\left(V_{refU}+V_{refL}\right)$

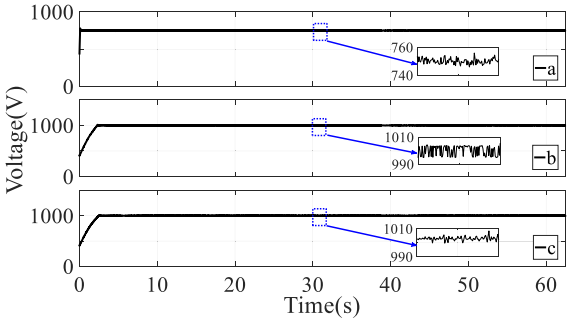

FIGURE 20. DC link voltage, (a) BB, (b) NS, and (c) FL converters.

optimal performance zone, the ICE surplus torque is stored in the battery through the inner rotor winding as energy. As it can be seen, due to use the higher DC-link voltage for NS and FL converters, the torque ripple of these converters are more than the BB ones. Fig. 19 shows all generated torques by ICE, stator, and wheels in one frame. As it can be deduced, the sum of the ICE torque and stator torque is equal to requested torque by the wheels. As shown in Fig. 20, the DC link voltages of three converters are constant and have small voltage ripple.

VII. CONCLUSION

In this paper, the DMPM and its placement in the structure of HEVs were firstly introduced. Then, with the introduction of the nine-switch and five-leg converters, modeling of complete system including the energy management unit is presented, followed by the control strategy and the space vector modulation schemes for different topologies. Finally, using a standard drive cycle, the performance of the DMPM-based HEV was investigated in the presence of three converters. The simulation results show that with the NS and the FL while reducing the overall size and the weight of the system by reducing the number of switches and their accessories, the vehicle follows the drive cycle as closely as a conventional BB converter. However, compared to the BB converter, higher DC-link voltage is required in these topologies in order to have same maximum achievable output voltages. It is found that the NS and FL converters might have less switching loss than BB converter depending on the current rating of the stator and inner rotor windings.

REFERENCES

[1] P. Y. Kong and G. K. Karagiannidis, "Charging schemes for plug-in hybrid electric vehicles in smart grid: A survey," *IEEE Access*, vol. 4, pp. 6846–6875, Nov. 2016.
[2] M. Ghanaatian and A. Radan, "Application and simulation of dual-mechanical-port machine in hybrid electric vehicles," *Int. Trans. Elect. Energy Syst.*, vol. 25, no. 3, pp. 1083–1099, Jun. 2014.
[3] A. Ghayebloo and A. Radan, "Superiority of dual-mechanical-port-machine-based structure for series–parallel hybrid electric vehicle applications," *IEEE Trans. Veh. Technol.*, vol. 65, no. 2, pp. 589–603, Feb. 2016.
[4] M. Asghar, A. I. Bhatti, Q. Ahmed, and G. Murtaza, "Energy management strategy for Atkinson cycle engine based parallel hybrid electric vehicle," *IEEE Access*, vol. 6, pp. 28008–28018, May 2010.
[5] Y. Wang, S. Niu, and W. Fu, "Electrical-continuously variable transmission system based on doubly fed flux-bidirectional modulation," *IEEE Trans. Ind. Electron.*, vol. 64, no. 6, pp. 2722–2731, Apr. 2016.
[6] Y. Liu, S. L. Ho, W. N. Fu, and Z. Zhang, "Design optimization of a novel doubly fed dual-rotor flux-modulated machine for hybrid electric vehicles," *IEEE Trans. Magn.*, vol. 51, no. 3, Mar. 2015, Art. no. 8101604.
[7] L. Xu, "A new breed of electric machines—Basic analysis and applications of dual mechanical port electric machines," in *Proc. 8th Int. Conf. Elect. Mach. Syst.*, vol. 1, Sep. 2005, pp. 24–31.
[8] E. Vinot, R. Trigui, Y. Cheng, C. Espanet, A. bouscayrol, and V. Reinbold, "Improvement of an EVT-based HEV using dynamic programming," *IEEE Trans. Veh. Technol.*, vol. 63, no. 1, pp. 40–51, Jan. 2014.
[9] E. Vinot, V. Reinbold, and R. Trigui, "Global optimized design of an electric variable transmission for HEVs," *IEEE Trans. Veh. Technol.*, vol. 65, no. 8, pp. 6794–6798, Aug. 2016.
[10] H. Cai and L. Xu, "Modeling and control for cage rotor dual mechanical port electric machine—Part I: Model development," *IEEE Trans. Energy Convers.*, vol. 30, no. 3, pp. 957–965, Sep. 2015.
[11] H. Cai and L. Xu, "Modeling and control for cage rotor dual mechanical port electric machine—Part II: Independent control of two rotors," *IEEE Trans. Energy Convers.*, vol. 30, no. 3, pp. 966–974, Sep. 2015.
[12] J. Druant, H. Vansompel, F. De Belie, and P. Sergeant, "Optimal control for a hybrid excited dual mechanical port electric machine," *IEEE Trans. Energy Convers.*, vol. 32, no. 2, pp. 599–607, Jun. 2017.
[13] Z. Xiang, L. Quan, X. Zhu, and L. Wang, "A brushless double mechanical port permanent magnet motor for plug-In HEVs," *IEEE Trans. Magn.*, vol. 51, no. 11, Nov. 2015, Art. no. 8111104.
[14] J. Bai, P. Zheng, C. Tong, Z. Song, and Q. Zhao, "Characteristic analysis and verification of the magnetic-field-modulated brushless double-rotor machine," *IEEE Trans. Ind. Electron.*, vol. 62, no. 7, pp. 4023–4034, Jul. 2015.
[15] P. Zheng, J. Bai, C. Tomg, Y. Sui, Z. Song, and Q. Zhao, "Investigation of a novel radial magnetic-field-modulated brushless double-rotor machine used for HEVs," *IEEE Trans. Magn.*, vol. 49, no. 3, pp. 1231–1241, Mar. 2013.
[16] Y. Yang, N. Schofield, and A. Emadi, "Double-rotor switched reluctance machine (DRSRM)," *IEEE Trans. Energy Convers.*, vol. 30, no. 2, pp. 671–681, Jun. 2015.

[17] J. L. Sanz *et al.*, "Nonlinear model predictive control for thermal management in plug-in hybrid electric vehicles," *IEEE Trans. Veh. Technol.*, vol. 66, no. 5, pp. 3632–3644, May 2017.
[18] J. Lopez-Sanz *et al.*, "Thermal management in plug-in hybrid electric vehicles: A real-time nonlinear model predictive control implementation," *IEEE Trans. Veh. Technol.*, vol. 66, no. 9, pp. 7751–7761, Sep. 2017.
[19] M. Roche, W. Shabbir, and S. A. Evangelou, "Voltage control for enhanced power electronic Efficiency in series hybrid electric vehicles," *IEEE Trans. Veh. Technol.*, vol. 66, no. 5, pp. 3645–3658, May 2017.
[20] S. Stockar, V. Marano, M. Canova, G. Rizzoni, and L. Guzzella, "Energy-optimal control of plug-in hybrid electric vehicles for real-world driving cycles," *IEEE Trans. Veh. Technol.*, vol. 60, no. 7, pp. 2949–2962, Sep. 2011.
[21] E. Mese, Y. Yasa, H. Akca, M. G. Aydeniz, and M. Garip, "Investigating operating modes and converter options of dual winding permanent magnet synchronous machines for hybrid electric vehicles," *IEEE Trans. Energy Convers.*, vol. 30, no. 1, pp. 285–295, Mar. 2015.
[22] M. Amrhein and P. T. Krein, "Dynamic simulation for analysis of hybrid electric vehicle system and subsystem interactions, including power electronics," *IEEE Trans. Veh. Technol.*, vol. 54, no. 3, pp. 825–836, May 2005.
[23] S. M. Dehghan, M. Mohamadian, and A. Yazdian, "Hybrid electric Vehicle based on bidirectional Z-source nine-switch inverter," *IEEE Trans. Veh. Technol.*, vol. 59, no. 6, pp. 2641–2653, Jul. 2010.
[24] X. Chen, T. Pang, S. Huang, and S. Wan, "Control of the dual mechanical port electrical machine and its applications in hybrid electrical vehicle," *IEEJ Trans. Elect. Electron. Eng.*, vol. 8, no. 1, pp. 94–100, Jan. 2013.
[25] L. Xu, Y. Zhang, and X. Wen, "Multioperational modes and control strategies of dual-mechanical-port machine for hybrid electrical vehicles," *IEEE Trans. Ind. Appl.*, vol. 45, no. 2, pp. 747–756, Mar. 2009.
[26] C. S. Lim, N. A. Rahim, W. P. Hew, and E. Levi, "Model predictive control of a two-motor drive with five-leg-inverter supply," *IEEE Trans. Ind. Electron.*, vol. 60, no. 1, pp. 54–66, Jan. 2013.
[27] D. Zhou, J. Zhao, and Y. Li, "Model-predictive control scheme of five-leg AC–DC–AC converter-fed induction motor drive," *IEEE Trans. Ind. Electron.*, vol. 63, no. 7, pp. 4517–4526, Jul. 2016.
[28] A. Ghayebloo and A. Radan, "Maximum torque per ampere (MTPA) control of dual mechanical ports electric machine," in *Proc. PEDSTC*, Feb. 2010, pp. 249–254.
[29] W. L. Soong and N. Ertugrul, "Field-weakening performance of interior permanent-magnet motors," *IEEE Trans. Ind. Appl.*, vol. 38, no. 5, pp. 1251–1258, Sep./Oct. 2002.
[30] Q. Wang and S. Niu, "A novel hybrid-excited dual-PM machine with bidirectional flux modulation," *IEEE Trans. Energy Convers.*, vol. 32, no. 2, pp. 424–435, Jun. 2017.
[31] X. Sun and M. Cheng, "Thermal analysis and cooling system design of dual mechanical port machine for wind power application," *IEEE Trans. Ind. Electron.*, vol. 60, no. 5, pp. 1724–1733, May 2013.
[32] K. Ali, P. Das, and S. K. Panda, "A special application criterion of the nine-switch converter with reduced conduction loss," *IEEE Trans. Ind. Electron.*, vol. 65, no. 4, pp. 2853–2862, Apr. 2018.
[33] S. M. D. Dehnavi, M. Mohamadian, A. Yazdian, and F. Ashrafzadeh, "Space vectors modulation for nine-switch converters," *IEEE Trans. Power Electron.*, vol. 25, no. 6, pp. 1488–1496, Jun. 2010.
[34] A. Khodadoost and A. Radan, "Novel comparative study between SVM, DTC and DTC-SVM in Five-Leg Inverter to drive two motors independently," in *Proc. PEDSTC*, 2013, pp. 294–300.
[35] M. Hamouda, H. F. Blanchette, and K. Al-Haddad, "A hybrid modulation scheme for dual-output five-leg indirect matrix converter," *IEEE Trans. Ind. Electron.*, vol. 63, no. 12, pp. 7299–7309, Dec. 2016.
[36] Z. Qin, P. C. Loh, and F. Blaabjerg, "Application criteria for nine-switch power conversion systems with improved thermal performance," *IEEE Trans. Power Electron.*, vol. 30, no. 8, pp. 4608–4620, Aug. 2015.
[37] "Evaluation of 2004 toyota prius hybrid electric drive system," Oak Ridge Nat. Lab., Mitch Olszewski, U.S. Dept Energy, Washington, DC, USA, Tech. Rep. ORNL/TM-2006/423, May 2006. [Online]. Available: http://inspire.ornl.gov/OriginalDocument/f38948a5-d6a2-4f80-8cc9-34b77e3862a3

HAMED BIZHANI (S'17) was born in Mashhad, Iran, in 1988. He received the B.Sc. degree in electrical engineering from Birjand University, Birjand, Iran, in 2011, and the M.Sc. degree in electrical engineering from the K. N. Toosi University of Technology, Tehran, Iran, in 2013. He is currently pursuing the Ph.D. degree in electrical engineering with the University of Zanjan, Zanjan, Iran. He was a Visiting Research Associate with Curtin University, Perth, WA, Australia. His current research interests include multiport power electronic converters, control and integration of distributed generations, space vector modulation, and hybrid electric vehicle.

GANG YAO received the M.S. and Ph.D. degrees from the Electrical Engineering Department, Shanghai Maritime University, Shanghai, China, in 2003 and 2008, respectively. In 2008, he joined the Institut de Recherche en Communications et en Cybernétique de Nantes (IRCCyN), Nantes, France, as a Postdoctoral Research Fellow. Since 2009, he has been an Assistant Professor with the Electrical Engineering Department, Shanghai Maritime University. His current research interests include multi-agent-based intelligent control, fault diagnosis, and fault-tolerant control of microgrids and marine power systems.

S. M. MUYEEN (S'03–M'08–SM'12) received the B.Sc.Eng. degree from the Rajshahi Institute of Technology, Bangladesh, in 2000, and the M.Eng. and Ph.D. degrees from the Kitami Institute of Technology, Japan, in 2005 and 2008, respectively, all in electrical and electronic engineering. He is currently an Associate Professor with the Department of Electrical and Computer Engineering, Curtin University, Perth, WA, Australia. He has published more than 175 articles in different journals and international conferences. He has published six books as an author or an editor. His research interests include power system stability and control, electrical machine, FACTS, energy storage systems (ESS), renewable energy, and HVdc systems. He has been a Keynote Speaker and an Invited Speaker at many international conferences, workshops, and universities. He serves as an Editor/an Associate Editor for many prestigious journals from IEEE, IET, and other publishers, including the IEEE TRANSACTIONS OF SUSTAINABLE ENERGY, the IEEE POWER ENGINEERING LETTERS, *IET Renewable Power Generation*, and *IET Generation, Transmission and Distribution*. He is a Fellow of Engineers Australia.

SYED MOFIZUL ISLAM received the B.Sc. degree in electrical engineering from the Bangladesh University of Engineering and Technology, Bangladesh, in 1979, and the M.Sc. and Ph.D. degrees in electrical power engineering from the King Fahd University of Petroleum and Minerals, Dhahran, Saudi Arabia, in 1983 and 1988, respectively. Prior to joining Federation University, he was the John Curtin Distinguished Professor in electrical power engineering and the Director of the Centre for Smart Grid and Sustainable Power Systems, Curtin University, Perth, WA, Australia. He was the Dean of the Faculty of Science and Engineering, Curtin University, from 2011 to 2018. He has been a Visiting Professor with the Shanghai University of Electrical Power and Xi'an Jiatong University, China. He is currently the Dean of the School of Science Engineering and Information Technology, Federation University Australia. He has extensive experience in international collaboration in both education and research with institutes and researchers in China and other countries. His research interests include condition monitoring of transformers, wind energy conversion, and smart power systems. He has published over 270 technical papers in his area of expertise. He is a Fellow of the Engineers Australia and the IET, a Senior Member of IAS, PES, and DEIS, and a Chartered Engineer in U.K. and a Chartered Professional Engineer in Australia. He is a member of the Steering Committee of the Australian Power Institute and the WA EESA Board. He received the Dean's Medallion for research at Curtin University, in 1999, the IEEE T Burke Haye's Faculty Recognition Award, in 2000, the Curtin University Inaugural Award for Research Development, in 2012, and the Sir John Madsen Medal, in 2011 and 2014, for the Best Electrical Engineering Paper in Australia. He has been a Keynote Speaker and an Invited Speaker at many international workshops and conferences. He was the Guest Editor-in-Chief of the IEEE TRANSACTIONS ON SUSTAINABLE ENERGY, Special Issue on Variable Power Generation Integration into Grid. He is a Founding Editor of the IEEE TRANSACTIONS ON SUSTAINABLE ENERGY and an Associate Editor of the *IET Renewable Power Generation*.

LAZHAR BEN-BRAHIM (S'88–M'91–SM'02) received the B.Sc. and M.Sc. degrees in electrical engineering from the National School of Engineers of Tunis, Tunis, Tunisia, in 1985 and 1987, respectively, and the Ph.D. degree in electrical and computer engineering from Yokohama National University, Yokohama, Japan, in 1991. From 1991 to 1997, he was with Toshiba Corporation, Tokyo, Japan. Since 1997, he has been with Qatar University, where he is currently a Full Professor with the Department of Electrical Engineering. He was the Industrial Electronics Chair with RasGas Company, the Head of the Industrial Technology Department, and the Head of the Department of Electrical Engineering. He has authored more than 130 journal/conference papers and book chapters. He holds more than 10 international patents. His research interests include power electronics, electric drives, renewable energy, control applications, and sensors/instrumentation. He is a member of the Institute of Electrical Engineers of Japan.